



SYNTHESIS, STRUCTURAL AND PHOTO LUMINESCENT PROPERTIES OF $\text{Li}_3\text{Ba}_2\text{Gd}_3(\text{MoO}_4)_8: \text{RE}^{3+}$ (RE= Pr^{3+} , Sm^{3+}) RED PHOSPHORS

SHASHI B PANDEY ^a *, CHITRA S KHADE ^a , APARNA J NADGOWDA ^a
^a Department of Physics, G H Rasoni University, Amravati 444701, India

ABSTRACT:

Many potential lighting applications have been proposed for Pr^{3+} and Sm^{3+} activated phosphor materials due to their emission (4f - 4f transitions). Pr^{3+} ions emit distinct radiation signatures depending on the host they are paired with. In the visible spectrum, Pr^{3+} ions emit radiation from the $^1\text{D}_2$ level, $^3\text{P}_0$ level, $^1\text{S}_0$ level, and UV level due to their 4f₂ electronic arrangement (from the 4f - 5d state). Sm^{3+} ions glow intensely in the orange-red region of the visible spectrum due to their 4f₅ electrical configuration. Both $\text{Li}_3\text{Ba}_2\text{Gd}_3(\text{MoO}_4)_8:\text{xPr}^{3+}$ (x = 0.01, 0.03, 0.05, 0.07, and 0.09 mol) and $\text{Li}_3\text{Ba}_2\text{Gd}_3(\text{MoO}_4)_8:\text{xSm}^{3+}$ (x = 0.01, 0.03, 0.05, 0.07, and 0.09 mol) were synthesized and their luminescent characteristics are reported here using the microwave-assisted SSM technique. The produced samples' optical and structural properties were further investigated.

Keywords: Luminescent, material, Red, Phosphors, SSM.

DOI Number: 10.14704/nq.2022.20.10.NQ55675

NeuroQuantology 2022;20(10):6798-6810

INTRODUCTION:

The practical use of rare earth elements in catalysts, magnets, brilliant phosphors, and other beneficial technologies have led to an explosion in research into these elements in recent years. Recently, research has been done on phosphors, which emit light on their own. There are several uses for white light emitting diodes (w-LEDs), including electronic displays (such TVs and computers), radiation detectors, imaging live objects, and lasers in certain kinds of medical equipment [1-3]. The various advantages of W-LEDs over traditional light

sources like incandescent bulbs and fluorescent tubes have led to their rapid rise in popularity in recent years. Doping host materials with rare earth ions for use in white LEDs has motivated research into their spectrum features [4-6]. The broad use of fluorescent lighting and other phosphor-related goods has resulted in substantial consumption of these resources by the lighting sector. The simplicity with which these phosphor-coated lamps may be manufactured is a major boon to the company. Methods based on the use of primary excitation energy to generate luminescence in inorganic host materials are often applied when



investigating the effectiveness of rare-earth luminescence. The energy is transferred from the excitation to the host lattice, then to the activator, then to the neighbors, and finally to the activator as light. [7].

Due to its peculiar energy level distribution, the Pr^{3+} ion in the [Xe] $4f^2$ structure is an uncommon activator for phosphors [8]. By bouncing between energy levels, the Pr^{3+} ion may be able to generate light spanning the visible to infrared spectrum [9]. Diverse host materials were used to create the different Pr^{3+} -doped phosphors, such as $\text{CaTiO}_3:\text{Pr}^{3+}$ [11], $\text{BaMoO}_4:\text{Pr}^{3+}$ [12] and $\text{LaMgAl}_{11}\text{O}_{19}:\text{Pr}^{3+}$ [13]. If the Pr^{3+} ion could be doped into a host material that can create green and red lights simultaneously, then exciting the blue light chip might yield pure white light. This might be quite useful when paired with w-LEDs [14].

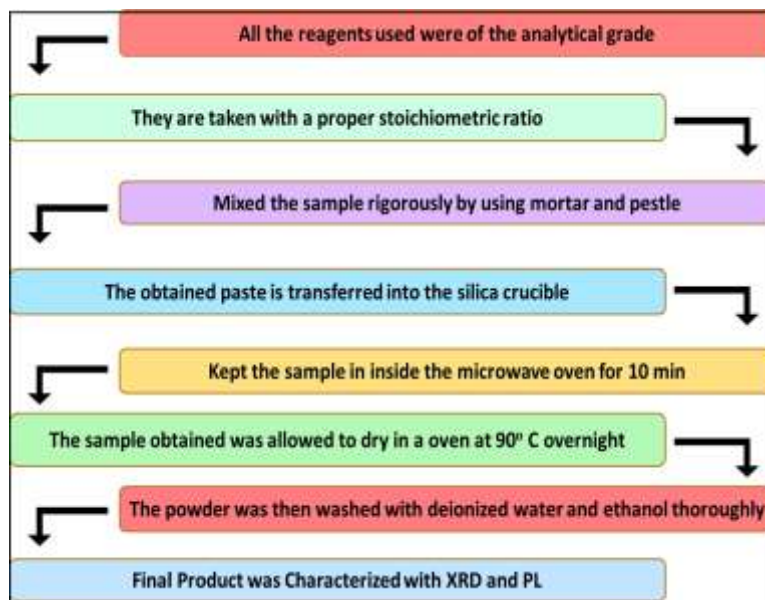
The Pr^{3+} ion, in contrast to other rare earth ions, has a complex energy level scheme, allowing it to emit light throughout a broad spectrum, from the visible to the near-infrared [15]. Since the red phosphor $\text{CaTiO}_3:\text{Pr}^{3+}$ was reported by Diallo [16] in 1997, a great deal of investigation has gone into Pr^{3+} activated phosphors, and other host lattices have demonstrated diverse emission colors for these materials. $\text{Gd}_2\text{O}_3:\text{Pr}^{3+}$ is highly luminescent in the green region of the spectrum [17], while $\text{BaMoO}_4:\text{Pr}^{3+}$ emits mostly red light. This means that by doping Pr^{3+} ions into suitable host materials, high-quality luminescent phosphor compounds may be produced.

Herein, we provide a preliminary report on the fabrication of Pr^{3+} -doped $\text{Li}_3\text{Ba}_2\text{Gd}_3(\text{MoO}_4)_8$ by microwave metathesis. Metathesis reactions in solids are exceedingly rare. This microwave-assisted synthesis procedure produces a crystalline product with diverse microstructures in a short period of time and leaves behind a byproduct that can be readily washed away with water.

Experimental process:

A series of $\text{Li}_3\text{Ba}_2\text{Gd}_3(\text{MoO}_4)_8: x\text{Pr}^{3+}$ ($x = 0.01$ and 0.09 mol) and $\text{Li}_3\text{Ba}_2\text{Gd}_3(\text{MoO}_4)_8: x\text{Sm}^{3+}$ ($x = 0.01$ and 0.09 mol) phosphors were prepared via microwave-assisted solid-state metathesis. Analytical-grade Lithium Nitrate- LiNO_3 , Barium Nitrate, $\text{Gd}(\text{NO}_3)_3 \cdot 6\text{H}_2\text{O}$, $(\text{NH}_4)_6\text{Mo}_7\text{O}_{24} \cdot 24\text{H}_2\text{O}$ and Pr_2O_3 used as starting materials for the preparation of $\text{Li}_3\text{Ba}_2\text{Gd}_3(\text{MoO}_4)_8: x\text{Pr}^{3+}$. They are combined in the right stoichiometric ratio in a mortar and pestle. First, a paste is prepared by crushing the sample using a mortar and pestle, and then it is added to a silica crucible. Next, we heated the powdered sample for 10 minutes in a microwave. Once the reaction was finished, the powder was washed with deionized water and ethanol before being dried in an oven at 90°C for a whole night. Once it reached room temperature, it was taken out. As soon as the sample has cooled, it is reground in an agate mortar and put to use in the laboratory. Lithium Nitrate- LiNO_3 , Barium Nitrate, $\text{Gd}(\text{NO}_3)_3 \cdot 6\text{H}_2\text{O}$, $(\text{NH}_4)_6\text{Mo}_7\text{O}_{24} \cdot 24\text{H}_2\text{O}$ and high-purity Sm_2O_3 and all of them were of the analytical grade.





Structural analysis:

The XRD patterns of a few of the samples we looked at are shown in Figure 1. $\text{Li}_3\text{Ba}_2\text{Gd}_3(\text{MoO}_4)_8$ experimental peaks are demonstrated to be in good agreement with the standard data (JCPDS. No. 77-0830). The XRD spectra show well defined peaks, indicating that a single crystalline phase of $\text{Li}_3\text{Ba}_2\text{Gd}_3(\text{MoO}_4)_8$ with space group $C2/c$ has been successfully synthesized. The crystal structure of $\text{Li}_3\text{Ba}_2\text{Gd}_3(\text{MoO}_4)_8$ was reported by Klevtsova et al. at [19]. In Figure 1 we see an example of an a-axis unit cell (a). The crystal structure includes two separate molybdenum

$$D = 0.9 \lambda / \beta \cos \theta$$

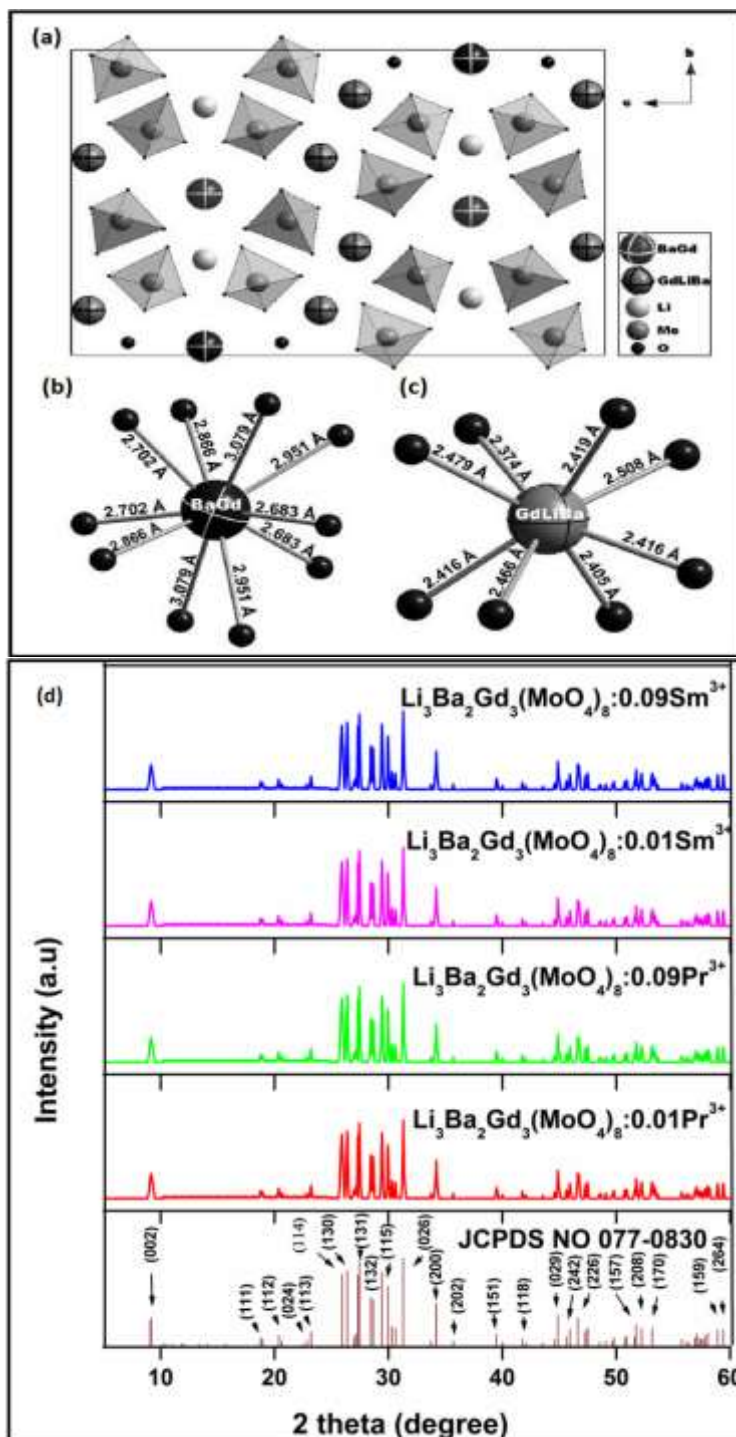
where, D is denoted as the average grain size, λ represents $\text{CuK}\alpha$ wavelength 0.1542 nm and β indicates the FWHM of the peak at Bragg angle θ . The calculated average crystallite size is

ions, each of which is tetrahedrally coordinated. Figure 1(b) shows that the barium ion is at a special place on the 2-fold axis, coordinated by 10 oxygen anions. More than two-thirds of the Li ions are in deformed octahedral coordination, while the rest of the ions are coordinatively close to Ba^{2+} and Gd^{3+} ions in an 8-fold coordination scheme (c).

By determining the size of the product's most intense peak, we may get a sense of its approximate crystallite size (131). Here is the formula for particle size according to the Debye-Scherrer equation,

about 87 nm for $\text{Li}_3\text{Ba}_2\text{Gd}_3(\text{MoO}_4)_8$: xPr^{3+} ($x = 0.01$ and 0.09 mol) and is about 63 nm for $\text{Li}_3\text{Ba}_2\text{Gd}_3(\text{MoO}_4)_8$: xSm^{3+} ($x = 0.01$ and 0.09 mol) respectively.”.





6801

Figure 1: (a) “The a-axis of a unit cell of $\text{Li}_3\text{Ba}_2\text{Gd}_3(\text{MoO}_4)_8$.”, (b) “Ba,Gd site with CN = 10” (c) “Gd,Li,Ba site with CN = 8 ” and (d)” “ Powder XRD patterns of $\text{Li}_3\text{Ba}_2\text{Gd}_3(\text{MoO}_4)_8$: $x\text{Pr}^{3+}$ ($x = 0.01$ and 0.09 mol) and $\text{Li}_3\text{Ba}_2\text{Gd}_3(\text{MoO}_4)_8$: $x\text{Sm}^{3+}$ ($x = 0.01$ and 0.09 mol)”.

The powders of $\text{Li}_3\text{Ba}_2\text{Gd}_3(\text{MoO}_4)_8$ and $\text{Li}_3\text{Ba}_2\text{Gd}_3(\text{MoO}_4)_8:0.09\text{Pr}^{3+}$ were analyzed using scanning electron micrographs. The obtained

scanning electron micrographs are shown in Figure 2(a) and (b). Particles that are 3-5 μm in size and irregular in shape tend to aggregate,



and these larger particles are surrounding by smaller particles in the morphologies (about 500 nm). Despite this, no noticeable alterations were seen in scanning electron micrographs of the materials at varying Pr^{3+} concentrations.

Producing such large particles at such a low sintering temperature may be attributed to the high Li content in the structure, which fosters particle growth.

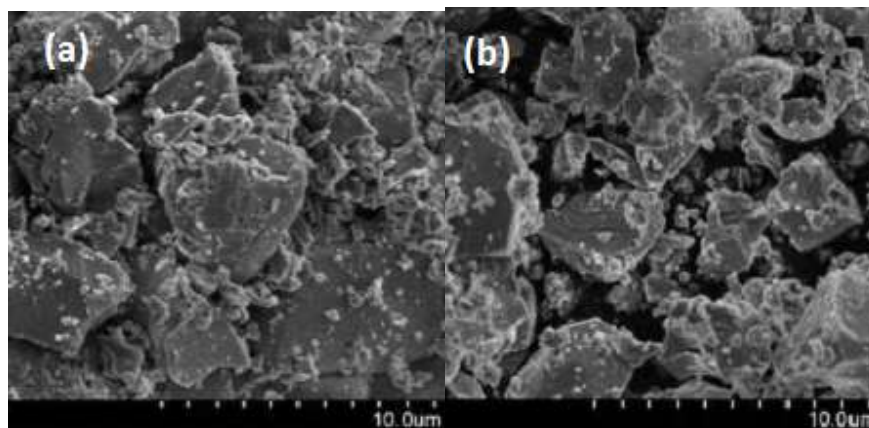


Figure 2: “SEM pictures of (a) $\text{Li}_3\text{Ba}_2\text{Gd}_3(\text{MoO}_4)_8$ and (b) $\text{Li}_3\text{Ba}_2\text{Gd}_3(\text{MoO}_4)_8:0.09\text{Pr}^{3+}$ under magnification of 5.0k”

Photoluminescence properties:

$\text{Li}_3\text{Ba}_2\text{Gd}_3(\text{MoO}_4)_8:x\text{Pr}^{3+}$ ($x= 0.01, 0.03, 0.05, 0.07$ and 0.09 mol) phosphor excitation and emission spectra are shown in Figure 3. Excitation spectra are monitored at an emission wavelength of 645 nm for $\text{Li}_3\text{Ba}_2\text{Gd}_3(\text{MoO}_4)_8:x\text{Pr}^{3+}$ ($x= 0.01, 0.03, 0.05, 0.07$ and 0.09 mol) With a peak at 294 nm, the excitation spectrum is powerful and highly adjustable thanks to a charge transfer transition

in the host. In addition to the CTB, a few thin absorption lines coming from 4f-4f shell transitions of Pr^{3+} ions may be seen in the spectral region about 450-500 nm. Maximum excitation occurs at a wavelength of 453 nm because Pr^{3+} ions undergo their typical f-f transitions., and the excitation bands consist of three primary peaks at ($^3\text{H}_4 \rightarrow ^3\text{P}_2$), 474 nm ($^3\text{H}_4 \rightarrow ^3\text{P}_1+^1\text{I}_6$) and 487 nm ($^3\text{H}_4 \rightarrow ^3\text{P}_0$)



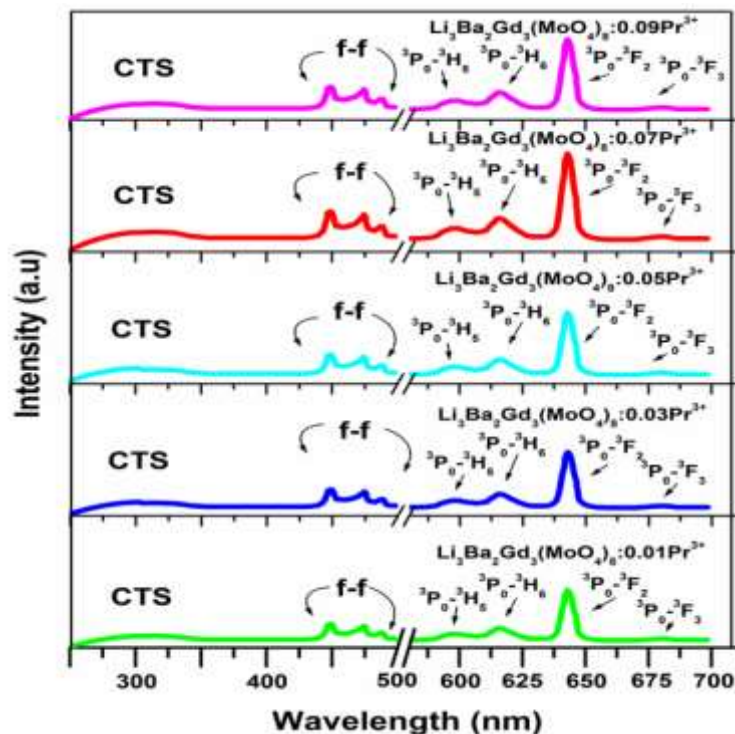


Figure 3: “The PLE ($\lambda_{em} = 645 \text{ nm}$) spectra and PL ($\lambda_{ex} = 450 \text{ nm}$) spectra of $\text{Li}_3\text{Ba}_2\text{Gd}_3(\text{MoO}_4)_8$: $x\text{Pr}^{3+}$ ($x = 0.01, 0.03, 0.05, 0.07$ and 0.09 mol)”.

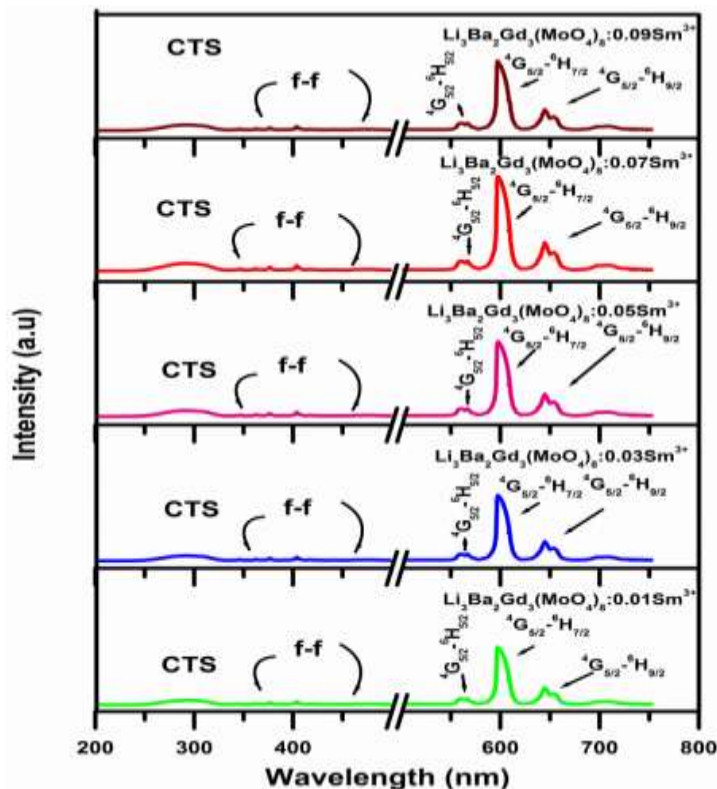
6803

At 594 nm (${}^3\text{P}_0 \rightarrow {}^3\text{H}_5$), 618 nm (${}^3\text{P}_0 \rightarrow {}^3\text{H}_6$), 645 nm (${}^3\text{P}_0 \rightarrow {}^3\text{F}_2$) and 680 nm (${}^3\text{P}_0 \rightarrow {}^3\text{F}_3$) the resultant emission spectrum displays four prominent emission peaks that correspond to the usual transitions of Pr^{3+} upon excitation at 453 nm. Pr^{3+} emits mostly in the red spectrum, with a peak at 645 nm (${}^3\text{P}_0 \rightarrow {}^3\text{F}_2$) red emission is the characteristic emission of Pr^{3+}). The PL spectra revealed that the phosphors' relative emission intensity rose with increasing doping concentration, peaking at $x = 0.07 \text{ mol}$. Concentration quenching causes the phosphor's emission intensity to diminish when more Pr^{3+} is added.

Figure 4 displays the excitation spectrum at the emission wavelength of 605 nm for phosphors $\text{Li}_3\text{Ba}_2\text{Gd}_3(\text{MoO}_4)_8$: $x\text{Sm}^{3+}$ ($x = 0.01, 0.03, 0.05,$

0.07 and 0.09 mol) synthesized using the microwave aided SSM reaction technique. The charge transfer transition in the host causes a wide band in the excitation spectrum between 225 and 330 nm, while intra - 4f transitions of Sm^{3+} cause strong peaks between 330 and 500 nm. At 404 nm, the excitation wavelength, the emission spectrum is tracked. As a result of the 4f-4f transitions of Sm^{3+} , it displays three distinct lines at 570 nm (${}^4\text{G}_{5/2} \rightarrow {}^6\text{H}_{5/2}$), 605 nm (${}^4\text{G}_{5/2} \rightarrow {}^6\text{H}_{7/2}$) and 649 nm (${}^4\text{G}_{5/2} \rightarrow {}^6\text{H}_{9/2}$). The crisp lines have the strongest emission at 605 nm (red). Other transitions between 530 nm and 750 nm are also faint. The greatest emission is seen at $\text{Li}_3\text{Ba}_2\text{Gd}_3(\text{MoO}_4)_8$: $x\text{Sm}^{3+}$ ($x = 0.01, 0.03, 0.05, 0.07$ and 0.09 mol) concentration of 7 mol%.





6804

Figure. 4: “The PLE ($\lambda_{em} = 605 \text{ nm}$) spectra and the photoluminescence emission ($\lambda_{ex} = 404 \text{ nm}$) spectra of $\text{Li}_3\text{Ba}_2\text{Gd}_3(\text{MoO}_4)_8:x\text{Sm}^{3+}$ ($x = 0.01, 0.03, 0.05, 0.07$ and 0.09 mol)”.

Scanning electron micrographs (SEM) of produced $\text{Li}_3\text{Ba}_2\text{Gd}_3(\text{MoO}_4)_8:x\text{Sm}^{3+}$ ($x = 0.09 \text{ mol}$) are shown in Figure 4. (a). Granularity is formed by the aggregate of the surface's large and small particles. High-quality ceramics may

need more pressure and/or sintering temperature, however. However, the limited range for the sintering temperature is a direct result of the material's low melting point.

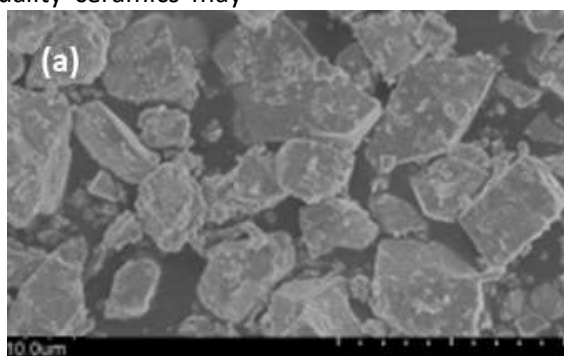


Figure. 4: (a) “SEM micrograph of $\text{Li}_3\text{Ba}_2\text{Gd}_3(\text{MoO}_4)_8:x\text{Sm}^{3+}$ ($x = 0.09 \text{ mol}$)”.

$\text{Li}_3\text{Ba}_2\text{Gd}_3(\text{MoO}_4)_8:0.07 \text{ Pr}^{3+}$, $\text{Li}_3\text{Ba}_2\text{Gd}_3(\text{MoO}_4)_8:0.07\text{Sm}^{3+}$, $\text{CaMoO}_4:\text{Eu}^{3+}$, $\text{Y}_2\text{O}_2\text{S}:\text{Eu}^{3+}$ phosphors are (0.687, 0.303), (0.603, 0.395), (0.678, 0.322) and (0.662, 0.334) respectively phosphors are shown in Figure 4

with their corresponding CIE chromaticity coordinates (x, y): (0.687, 0.303), (0.603, 0.395), (0.6 (b). The CIE diagram shows that when activated by a single wavelength ($\lambda_{ex} = 450 \text{ nm}$ and $\lambda_{ex} = 404 \text{ nm}$), the phosphor materials



synthesized from Pr and Sm doped $\text{Li}_3\text{Ba}_2\text{Gd}_3(\text{MoO}_4)_8$ display strong red emissions. Results show that red-emitting

$\text{Li}_3\text{Ba}_2\text{Gd}_3(\text{MoO}_4)_8:0.07\text{Pr}^{3+}$ and $\text{Li}_3\text{Ba}_2\text{Gd}_3(\text{MoO}_4)_8:0.07\text{Sm}^{3+}$ phosphors have potential for usage in White LEDs

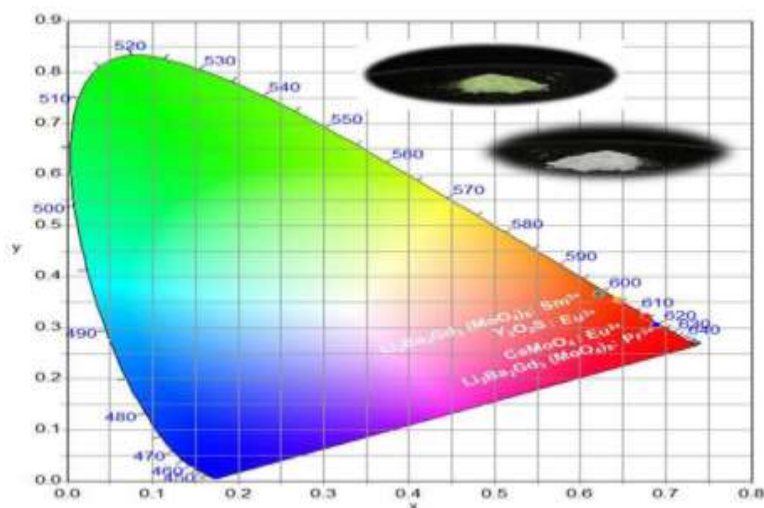
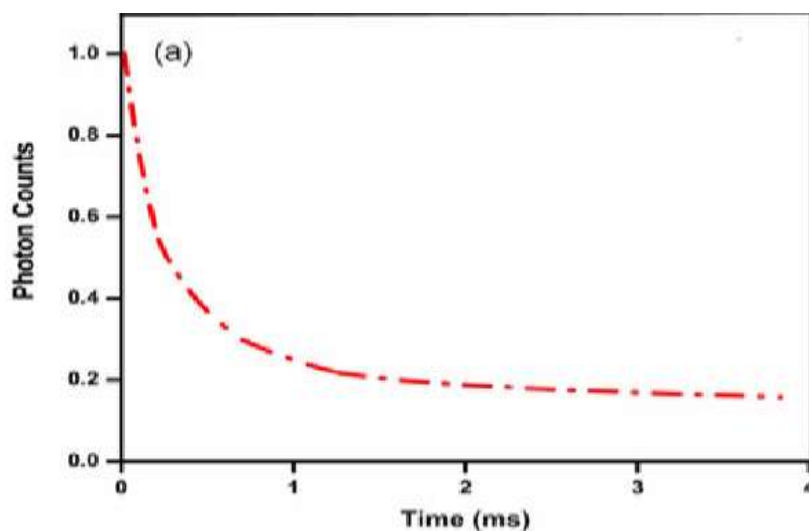


Figure. 4(b): “CIE chromaticity diagram for $\text{Li}_3\text{Ba}_2\text{Gd}_3(\text{MoO}_4)_8:0.07\text{Pr}^{3+}$, $\text{Li}_3\text{Ba}_2\text{Gd}_3(\text{MoO}_4)_8:0.07\text{Sm}^{3+}$, $\text{CaMoO}_4:\text{Eu}^{3+}$, $\text{Y}_2\text{O}_2\text{S}:\text{Eu}^{3+}$ phosphors”.

6805

The photoluminescence decay curves for the $\text{Li}_3\text{Ba}_2\text{Gd}_3(\text{MoO}_4)_8:0.07\text{Pr}^{3+}$, $\text{Li}_3\text{Ba}_2\text{Gd}_3(\text{MoO}_4)_8:0.07\text{Sm}^{3+}$ phosphors are shown in Figure 5(a) and Figure 6(a), respectively. The computed lifetimes of Pr^{3+} and Sm^{3+} are 0.321 ms and 0.310 ms, respectively, which may be fit by a single-exponential

function as $I = A \exp(-t/\tau)$ (τ is the life time of rare earth ion). In Figure 5(b) and Figure 6 we can see the typical particle size distribution of the optimized red-emitting phosphors (b). Particle size for $\text{Li}_3\text{Ba}_2\text{Gd}_3(\text{MoO}_4)_8:0.07\text{Sm}^{3+}$ is about 80 nm, whereas for $\text{Li}_3\text{Ba}_2\text{Gd}_3(\text{MoO}_4)_8:0.07\text{Pr}^{3+}$ it is around 60 nm.



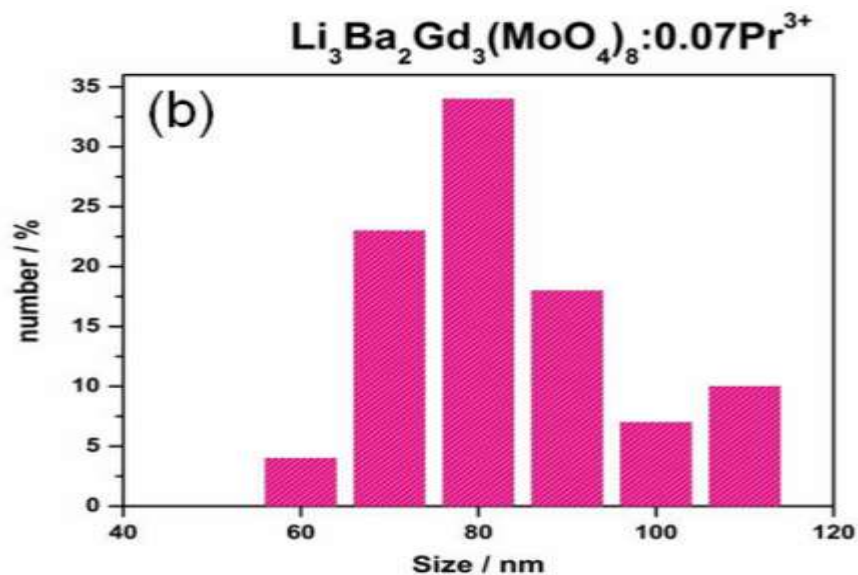
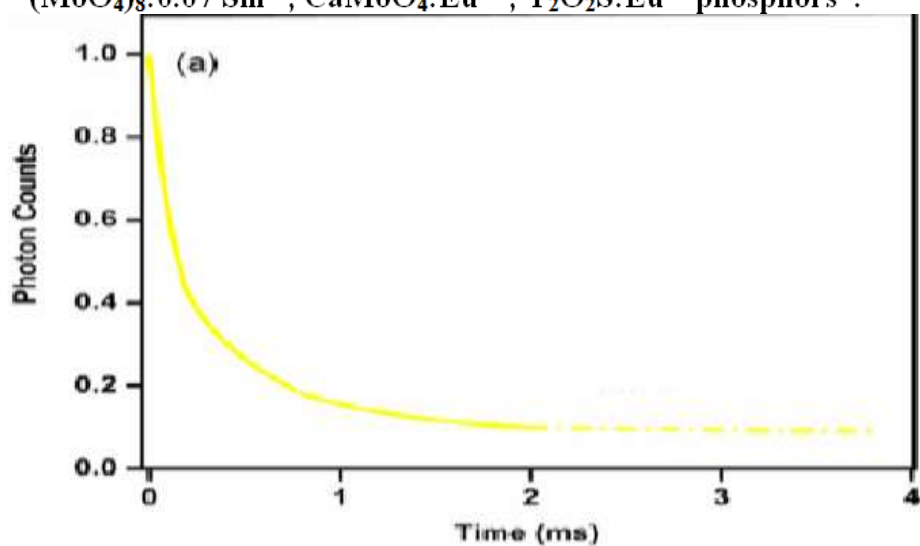
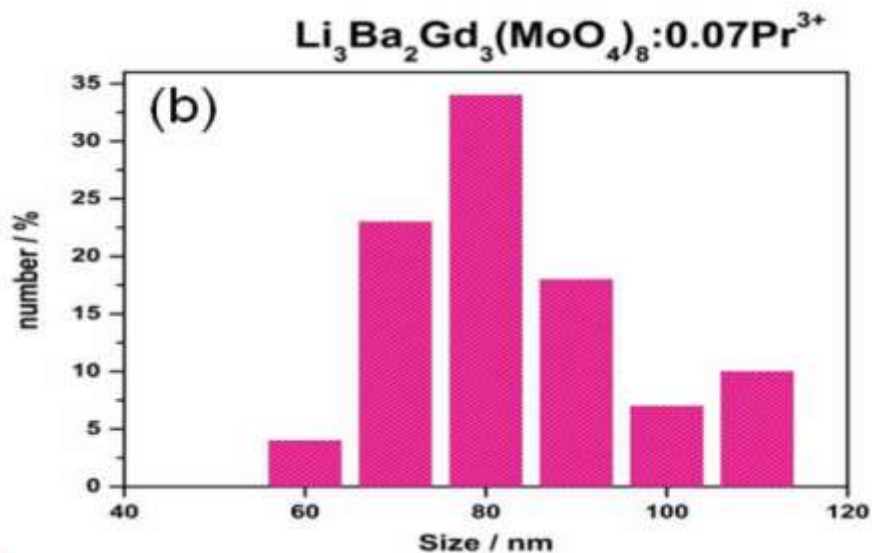


Figure. 4(b): “CIE chromaticity diagram for $\text{Li}_3\text{Ba}_2\text{Gd}_3(\text{MoO}_4)_8:0.07\text{Pr}^{3+}$, $\text{Li}_3\text{Ba}_2\text{Gd}_3(\text{MoO}_4)_8:0.07\text{Sm}^{3+}$, $\text{CaMoO}_4:\text{Eu}^{3+}$, $\text{Y}_2\text{O}_2\text{S}:\text{Eu}^{3+}$ phosphors”.

6806



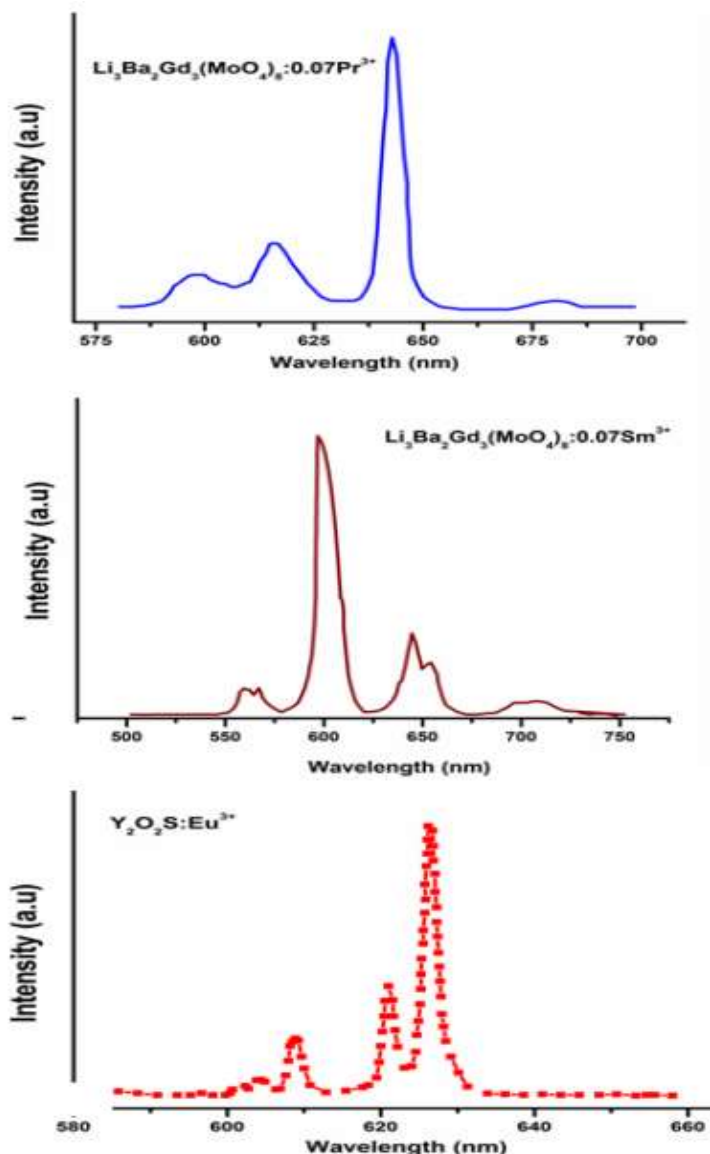


6807

Figure 6: (a) "Room temperature luminescent decay curve of $^4\text{G}_{5/2} \rightarrow ^6\text{H}_{7/2}$ transitions at 605 nm of Sm^{3+} ions of $\text{Li}_3\text{Ba}_2\text{Gd}_3(\text{MoO}_4)_8:0.07\text{Sm}^{3+}$ phosphor". (b) "Particle size distribution of $\text{Li}_3\text{Ba}_2\text{Gd}_3(\text{MoO}_4)_8:0.07\text{Sm}^{3+}$ ".

The current study compares the results of the emission spectra of the traditional red phosphor ($\text{Y}_2\text{O}_2\text{S}:\text{Eu}^{3+}$) manufactured by high temperature solid state reaction technique to those of the emission spectra of the work in progress. As seen in Figure 7, the PL spectra of various red phosphors are shown.





6808

Figure. 7: “Comparison of emission spectra of $\text{Li}_3\text{Ba}_2\text{Gd}_3(\text{MoO}_4)_8:0.07\text{Pr}^{3+}$, $\text{Li}_3\text{Ba}_2\text{Gd}_3(\text{MoO}_4)_8:0.07\text{Sm}^{3+}$ and $\text{Y}_2\text{O}_2\text{S}:\text{Eu}^{3+}$ phosphors”.

Specifically, it shows that the red emission intensity of $\text{Li}_3\text{Ba}_2\text{Gd}_3(\text{MoO}_4)_8:0.07\text{Pr}^{3+}$ and $\text{Li}_3\text{Ba}_2\text{Gd}_3(\text{MoO}_4)_8:0.07\text{Sm}^{3+}$ phosphors are on par with that of commercial ($\text{Y}_2\text{O}_2\text{S}:\text{Eu}^{3+}$) red phosphor. As well as $\text{Li}_3\text{Ba}_2\text{Gd}_3(\text{MoO}_4)_8:0.07\text{Pr}^{3+}$ is also present. An exciting new red-emitting material for WLEDs is 0.07Sm^{3+} phosphors, which can be generated by the microwave-assisted SSM reaction pathway.

CONCLUSION:

A simple microwave-assisted SSM reaction approach was used to successfully manufacture $\text{Li}_3\text{Ba}_2\text{Gd}_3(\text{MoO}_4)_8:\text{RE}^{3+}$ ($\text{RE}^{3+} = \text{Pr}^{3+}, \text{Sm}^{3+}$) phosphors. At a blue wavelength of 450 nm, $\text{Li}_3\text{Ba}_2\text{Gd}_3(\text{MoO}_4)_8$ undergoes excitation. With 0.07 mol Pr^{3+} phosphor, a strong red emission was seen at 645 nm. We have found that 7 mol% Pr^{3+} content in $\text{Li}_3\text{Ba}_2\text{Gd}_3(\text{MoO}_4)_8$ is the optimum doping concentration. When



activated by near-UV light, $\text{Li}_3\text{Ba}_2\text{Gd}_3(\text{MoO}_4)_8$ emits a luminous glow (404 nm). In particular, the 605 nm red emission lines were quite noticeable in 0.07mol Sm^{3+} phosphor. The optimum doping concentration of Sm^{3+} in $\text{Li}_3\text{Ba}_2\text{Gd}_3(\text{MoO}_4)_8$ is 8 mol% for which the red emission of $\text{Li}_3\text{Ba}_2\text{Gd}_3(\text{MoO}_4)_8:0$ is high intensity. The intensity of conventional $\text{Y}_2\text{O}_3:\text{Eu}^{3+}$ and the $\text{Pr}^{3+}, \text{Sm}^{3+}$ doped $\text{Li}_3\text{Ba}_2\text{Gd}_3(\text{MoO}_4)_8$ are comparable. According to all of the aforementioned findings, $\text{Li}_3\text{Ba}_2\text{Gd}_3(\text{MoO}_4)_8:0.07\text{Pr}^{3+}$ and $\text{Li}_3\text{Ba}_2\text{Gd}_3(\text{MoO}_4)_8:0.07\text{Sm}^{3+}$ phosphors are effective red emitting phosphors in near-UV/blue light GaN based White LEDs.

REFERENCES:

- Xia, Mao & Chen, Zhi&Gao, Peixing&Hintzen, Hubertus & Wong, Wai-Yeung & Wang, Jing & Zhou, Zhi. (2020). Pyrophosphate Phosphor Solid Solution with High Quantum Efficiency and Thermal Stability for Efficient LED Lighting. *iScience*. 23. 100892. 10.1016/j.isci.2020.100892.
- S.-J. Park, C.-H. Park, B.-Y. Yu, H.-S. Bae, C.-H. Kim, and C.-H. Pyun, "Structure and luminescence of $\text{SrY}_2\text{O}_4:\text{Eu}$," *Journal of the Electrochemical Society*, vol. 146, no. 10, pp. 3903–3906, 1999.
- R. Atkins and A. L. Diaz, "Investigation of host-to-activator energy transfer and surface losses in $\text{SrY}_2\text{O}_4:\text{Eu}^{3+}$ under VUV excitation," *Journal of Luminescence*, vol. 128, no. 9, pp. 1463–1470, 2008.
- Li, Mengting& Jiao, Baoxiang. (2015). Synthesis and photoluminescence properties of $\text{ZnTiO}_3:\text{Eu}^{3+}$ red phosphors via sol-gel method. *Journal of Rare Earths*. 33. 10.1016/S1002-0721(14)60408-7.
- J. Wan, Z. Wang, X. Chen, L. Mu, and Y. Qu, "Shape-tailored photoluminescent intensity of red phosphor $\text{Y}_2\text{O}_3:\text{Eu}^{3+}$," *Journal of Crystal Growth*, vol. 284, no. 3-4, pp. 538–543, 2005.
- G. S. Ofelt, "Intensities of crystal spectra of rare-earth ions," *The Journal of Chemical Physics*, vol. 37, no. 3, article 511, 1962.
- N. Shanta Singh, R. S. Ningthoujam, G. Phaomei, S. D. Singh, A. Vinu, and R. K. Vatsa,

"Re-dispersion and film formation of GdVO_4 : Ln (Ln = Dy, Eu, Sm, Tm) nanoparticles: particle size and luminescence studies," *Dalton Trans.* **41**(15), 4404–4412 (2012).

- Chen H.L., Wei L.K., Chang Y.S. Characterizations of Pr^{3+} Ion-Doped LaVO_4 Phosphor Prepared Using a Sol-Gel Method. *J. Electron. Mater.* 2018;47:6649–6654. doi: 10.1007/s11664-018-6561-6.
- Zhang L.Z., Hu Z.S., Lin Z.B., Wang G.F. Growth and spectral properties of $\text{Nd}^{3+}:\text{LaVO}_4$ crystal. *J. Cryst. Growth*. 2004;260:460–463. doi: 10.1016/j.jcrysgro.2003.08.067.
- Wang X.J., Wang X.J., Wang Z.H., Zhu Q., Zhu G., Wang C., Xin S.Y., Li J.G. Photo/cathodoluminescence and stability of $\text{Gd}_2\text{O}_3:\text{Tb}$, Pr green phosphor hexagons calcined from layered hydroxide sulfate. *J. Am. Ceram. Soc.* 2018;101:5477–5486. doi: 10.1111/jace.15797.
- Zhi J., Chen A., Ju L.K. Long lasting phosphorescence behavior of Pr^{3+} -doped CaTiO_3 -based oxides. *Opt. Mater.* 2009;31:1667–1672. doi: 10.1016/j.optmat.2009.04.004.
- Thirumalai J., Chandramohan R., Ahamed M.B., Ezhilvizhian S., Vijayan T.A. Pr^{3+} doped BaMoO_4 octahedron to shuttle-like microcrystals: Synthesis and luminescence properties. *J. Mater. Sci-Mater. El.* 2012;23:325–333. doi: 10.1007/s10854-011-0415-9.
- Min X., Fang M.H., Huang Z.H., Liu Y.G., Tang C., Wu X.W. Synthesis and optical properties of Pr^{3+} -doped $\text{LaMgAl}_{11}\text{O}_{19}$ -A novel blue converting yellow phosphor for white light emitting diodes. *Ceram. Int.* 2015;41:4238–4242. doi: 10.1016/j.ceramint.2014.11.070.
- Xi J., Xi K., Sadhanala A., Zhang K.H.L., Li G.R., Dong H., Lei T., Yuan F., Ran C.X., Jiao B., et al. Chemical sintering reduced grain boundary defects for stable planar perovskite solar cells. *Nano Energy*. 2019;56:741–750. doi: 10.1016/j.nanoen.2018.11.021.
- W.J. Guo, Y.F. Lin, X.H. Gong, Y.J. Chen, Z.D. Luo, Y.D. Huang, Polarized spectral properties of



Pr^{3+} ions in $\text{NaGd}(\text{MO}_4)_2$ crystal, Appl. Phys. B 94 (2009) 155–163.

16. P.T. Diallo, P. Boutinaud, R. Mahiou, J.C. Cousseins, Red luminescence in Pr^{3+} -doped calcium titanates, Phys. Status Solidi A: Appl. Mater. Sci. 160 (1997) 255–263.

17. J.B. Lian, X.D. Sun, T. Gao, Preparation of $\text{Gd}_2\text{O}_3:\text{Pr}$ scintillation ceramics by pressureless reaction sintering method, J. Mater. Sci. Technol. 25 (2009) 254–258.

18. X.Y. Yang, J. Liu, H. Yang, X. Yu, Y. Guo, Y. Zhou, J. Liu, Synthesis and characterization of new red phosphors for white LED applications, J. Mater. Chem. 19 (2009) 3771–3774.

19. R. F. Klevtsova, A. D. Vasiliev, L. A. Glinskaya, A. I. Kruglik, N. M. Kozhevnikova and V. P. Korsun, Zh. Strukt. Khim., 1992, 33, 126–130.

6810

